Improving representation of tropical wetland methane emissions with CYGNSS inundation maps

Cynthia Gerlein-Safdi[1,2,*], A. Anthony Bloom[3], Genevieve Plant[1], Eric A. Kort[1], Christopher S. Ruf[1]

[1] Dept. of Climate and Space Sciences and Engineering, University of Michigan, Ann Arbor, MI, USA
[2] Climate and Ecosystem Sciences Division, Lawrence Berkeley National Laboratory, Berkeley, CA, USA
[3] Jet Propulsion Laboratory, California Institute of Technology, Pasadena, CA, USA
[*] Corresponding author and lead contact. Email: *cgerleinsafdi@lbl.gov*

ORCID:
CGS: 0000-0001-8160-6167
AAB: 0000-0002-1486-1499
GP: 0000-0003-1973-8243
EAK: 0000-0003-4940-7541
CSR: 0000-0002-5937-4483

Key points (3 max, 140 characters max)

- CYGNSS data is used to produce monthly maps of tropical wetlands at 0.01°. The maps are used to drive the WetCHARTs methane emission model.
- The seasonality of inundation-based model results lags two months behind the rainfall-based models and shows larger dry-season emission.
- CYGNSS-based estimates, consistent with independent observations, show higher emissions with larger variability than inundation-driven estimates.

Abstract (250 words max)

Wetlands are the single largest source of methane to the atmosphere and their emissions are expected to respond to a changing climate. Inaccuracy and uncertainty in inundation extent drives differences in modeled wetland emissions and impacts representation of wetland emissions on inter-annual and seasonal time frames. Existing wetland maps are based on optical or NIR satellite data obscured by clouds and vegetation, often leading to underestimates in wetlands extent, especially in the Tropics. Here, we present new inundation maps based on the CYGNSS satellite constellation, operating in L-band that is not impacted by clouds or vegetation, providing reliable observations through canopy and cloudy periods. We map the temporal and spatial dynamics of the Pantanal and Sudd wetlands, two of the largest wetlands in the world, using CYGNSS data and a computer vision algorithm. We link these inundation maps to methane fluxes via WetCHARTs, a global wetland methane emissions model ensemble. We contrast CYGNSS-modeled methane emissions with WetCHARTs standard runs that use monthly rainfall data from ERA5, as well as the commonly used SWAMPS wetland maps. We find that the CYGNSS-based inundation maps modify the methane emissions in multiple ways. The seasonality of inundation and methane emissions is shifted by two months because of the lag in wetland recharge following peak rainfall. Both inundation and methane emissions also respond non-linearly to wet-season precipitation totals, leading to large interannual variability in emissions. Finally, the annual magnitude of emissions is found to be greater than previously estimated.

Keywords (up to 6): CH_4, flood, GNSS-R, Pantanal, Sudd, WetCHARTs

1 Introduction

Methane is a potent greenhouse gas whose concentrations have been increasing at an accelerating rate over the past decade [Fletcher & Schaefer, 2019, Nisbet et al., 2019]. After a decade of near-equilibrium [Turner et al., 2019], the drivers of renewed growth are still debated. Main anthropogenic sources of methane include fossil fuels leakage during extraction and transport or their incomplete burning, landfills, ruminant livestock, rice paddies, and waste water treatment plants [Miller et al., 2013, Ciais et al., 2013]. Natural sources consist predominantly of biogenic emissions from wetlands, either seasonally or permanently inundated areas, with smaller contributions from termites and geological sources such as geothermal vents [Ciais et al., 2013]. Among all these, emissions from wetlands are both the largest and most uncertain source [Saunois et al., 2016, Saunois et al., 2020] and methane emissions from wetlands around the globe are predicted to increase significantly with climate change [Zhang et al., 2017b]. Boreal ecosystems have been a source of concern because climate change has rapidly transformed these ecosystems into methane emitters [Treat et al., 2018, Post et al., 2019]. However, tropical wetlands are both a much larger [Koffi et al., 2020] and more uncertain source in the global CH_4 balance [Turner et al., 2019], where even modest shifts in methane production can affect the global budget on either inter-annual or decadal time frames. The largest source of uncertainty in tropical wetland emissions comes from the lack of information about their extent [Bloom et al., 2017, Parker et al., 2020]. But to understand how tropical wetlands are affected by climate change-induced shifts in precipitation and temperature, it is crucial to first be able to accurately represent how they respond to interannual variability in these parameters [Zhang et al., 2017a, Parker et al., 2018]. Capturing year-to-year variations in their extent should therefore be of the highest importance, but so far, the few available datasets have all had significant shortcomings for this application.

Wetland mapping can be done from a variety of remote sensing platforms, from drones [Jeziorska, 2019] to airplanes [Zweig et al., 2015] and satellites [Zhang et al., 2017a]. However, with their regular return times, satellites are better suited to survey highly seasonal wetlands. Optical sensors such as Landsat or MODIS provide high resolution maps [Landmann et al., 2010, Pekel et al., 2016] but are obstructed by clouds and vegetation. Constructing a cloud-free map can require months of accumulated data, making this data ill-suited for the study of seasonal processes such as wetland inundation. In the Tropics, these disadvantages become real issues, since small waterbodies are often covered by dense vegetation and the rainy season can be associated with month-long periods of continuous cloud cover [Martins et al., 2018], biasing optical-based maps towards dry season water levels. Synthetic aperture radar (SAR) microwave instruments are capable of seeing through clouds and vegetation [Hess et al., 2015], but their long return times and narrow tracks requires that data be accumulated over extended periods of time, making it difficult for these instruments to track short-term phenomena. Recently, the combination of SAR data from Sentinel-1 with a classification algorithm showed promises for near-real time mapping of urban flooding [Shen et al., 2019], but Sentinel-1's frequency is too high for the sensor to see through vegetation and the method can therefore not be applied to tropical wetlands. These approaches will therefore all tend to underestimate maximum extent and fail to capture seasonal dynamics that may dictate large interannual variability in wetland emissions in response to climate drivers. Finally, the latest version of the Global Inundation Estimate from Multiple Satellites [Prigent et al., 2007, Prigent et al., 2020], GIEMS-2, combines passive microwave observations at 19 and 37 GHz with NDVI data to provide monthly wetland maps. Water under vegetation is presumably captured by the different polarization of the passive sensors and a two-dimensional linear mixture model, but the authors acknowledge that the signal from the high frequency sensors gets highly attenuated by vegetation, and that the linear mixture model often overcompensates, leading to high uncertainty for water under vegetation, a key issue for studying tropical wetlands. In addition, the passive sensors used lead to a rather coarse resolution of $0.25^\circ \times 0.25^\circ$ of the product, limiting the study of finer scale hydrological processes.

Global Navigation Satellite System Reflectometry (GNSS-R) instruments have received a lot of attention in recent years for the strong signal coming from inland waterbodies due to the coherent reflection they are associated with [Camps, 2020, Chew & Small, 2020, Wang & Morton, 2020]. Launched in December 2016 and the first science GNSS-R mission, the Cyclone Global Navigation Satellite System (CYGNSS) constellation of eight satellites [Ruf et al., 2018] combines the unique water-sensing abilities of GNSS-R with a short return time [Bussy-Virat et al., 2019], opening up new possibilities in the realm of short-term waterbody monitoring. While the footprint of a single CYGNSS sounding over land is of about 1 km $\times$ 3.5 km, the random track sampling method often requires to downgrade the spatial resolution in order to obtain a higher temporal resolution [Bussy-Virat et al., 2019]. Many different approaches are actively being developed to extract information on the position of waterbodies from CYGNSS data including thresholding of the signal-to-noise ratio (SNR) data [Chew et al., 2018, Morris et al., 2019], computer vision techniques [Gerlein-Safdi & Ruf, 2019], and signal coherency analysis [Loria et al., 2020, Al-Khaldi et al., 2020]. Thresholding techniques are likely underestimating the waterbody extent because vegetation can attenuate the SNR from wetlands under vegetation [Nghiem et al., 2017, Carreno-Luengo

et al., 2020, Park et al., 2020]. The coherency analysis technique goes beyond the SNR and decomposes the signal into its coherent and incoherent components. While this technique is still being developed, it promises to increase the spatial resolution of CYGNSS-based wetland maps. However, this method is computationally demanding and requires the aggregation of CYGNSS data over multiple months, making it inadequate for the study of fast-changing waterbodies.

Here we propose a new and enhanced analysis of CYGNSS SNR data applied to the whole three years of data combined with a computer vision algorithm initially presented in [Gerlein-Safdi & Ruf, 2019]. Wetland maps at $0.01^\circ \times 0.01^\circ$ resolution are produced on a monthly basis and assimilated into the WetCHARTs methane emissions model ensemble [Bloom et al., 2017]. Developed in 2017, WetCHARTs is a global wetland methane emission model ensemble for wetland emissions modeling [Mitchard, 2018, Ganesan et al., 2019, Turner et al., 2019, Parker et al., 2020]. WetCHARTs has the ability to directly assimilate dynamic wetland extent maps or to use a combination of static wetland maps and rainfall data to drive seasonal variations.

In this study, we demonstrate 1) the ability for CYGNSS data to provide high resolution monthly maps of wetlands and 2) the impact this new information has on both the timing and the magnitude of modeled methane emissions, especially when compared to model outputs driven by either rainfall data or other remotely sensed wetland maps. For this work, we focus on two specific wetlands: the Pantanal, located at the border between Brazil, Bolivia and Paraguay, and the South Sudanese Sudd wetland. The Pantanal is the largest wetland in the world and the largest single natural source of methane [Nisbet et al., 2019], contributing about 3.3 Tg CH_4/year [Marani & Alvalá, 2007] and representing almost 4% of the annual CH_4 emissions from wetlands. The Sudd wetland was recently pointed out as an underestimated and growing source of methane based on an analysis of column retrievals of atmospheric CH_4 data collected by the Japanese Greenhouse gases Observing Satellite (GOSAT) [Lunt et al., 2019, Pandey et al., 2020]. In Section 2, we will describe the CYGNSS data, the algorithm used to extract wetland features from the data, as well as the WetCHARTs model. In Section 3, we will present our findings that show that using CYGNSS-based inundation maps instead of rainfall-based ones leads to a shift in the timing and the magnitude of modeled methane emissions at both locations. We will also compare our results to the commonly used Surface WAter Microwave Product Series (SWAMPS) wetland maps [Schroeder et al., 2015, Jensen & Mcdonald, 2019]. Finally, in Section 4, we will discuss how these results are in agreement with data from both in-situ experiments and satellites. We end by discussing the possible implications of these results on future tropical wetland methane emission evaluations.

2 Methods

2.1 CYGNSS-based watermasks

2.1.1 CYGNSS data

Here we use the SNR of the level 1, version 2.1 CYGNSS data freely available from the Physical Oceanography Distributed Active Archive Center (https://podaac.jpl.nasa.gov/) to produce a surface reflectivity (SR) signal based on [Gerlein-Safdi & Ruf, 2019]: assuming coherent scattering [Chew & Small, 2018], the SNR is corrected for receiving and transmitting antenna gains, transmitted power level, and propagation loss from transmitter to specular point and specular point to receiver. The average of the 5% lowest data are removed to provide a range of variation in SR data that is comparable to the initial SNR range, as has been done in previous work [Chew et al., 2018, Gerlein-Safdi & Ruf, 2019] and oceans are removed using CYGNSS' QC flags.

The algorithm developed in [Gerlein-Safdi & Ruf, 2019] to transform SR maps into watermasks was based on the standard deviation of a pixel with respect to the average of the neighboring pixels. This method proved an appropriate technique to look at permanent water bodies such as large rivers and lakes, but it required the aggregation of data over a large period of time (one year of data was presented in [Gerlein-Safdi & Ruf, 2019]) in order to have enough samples within the area used for background estimation. This made it difficult to use this method for the study of seasonal hydrological processes. Here, we propose a similar, but different approach: instead of determining whether a pixel is inundated based on its value compared to the spatial distribution (mean and standard deviation) of a box around the pixel, we look at how a single pixel looks compared to the distribution of values for that same pixel over two and half years of CYGNSS data (June 2017 until December 2019), the entire dataset available at the time this study was conducted. Accuracy is expected to improve as more data is assimilated into the algorithm.

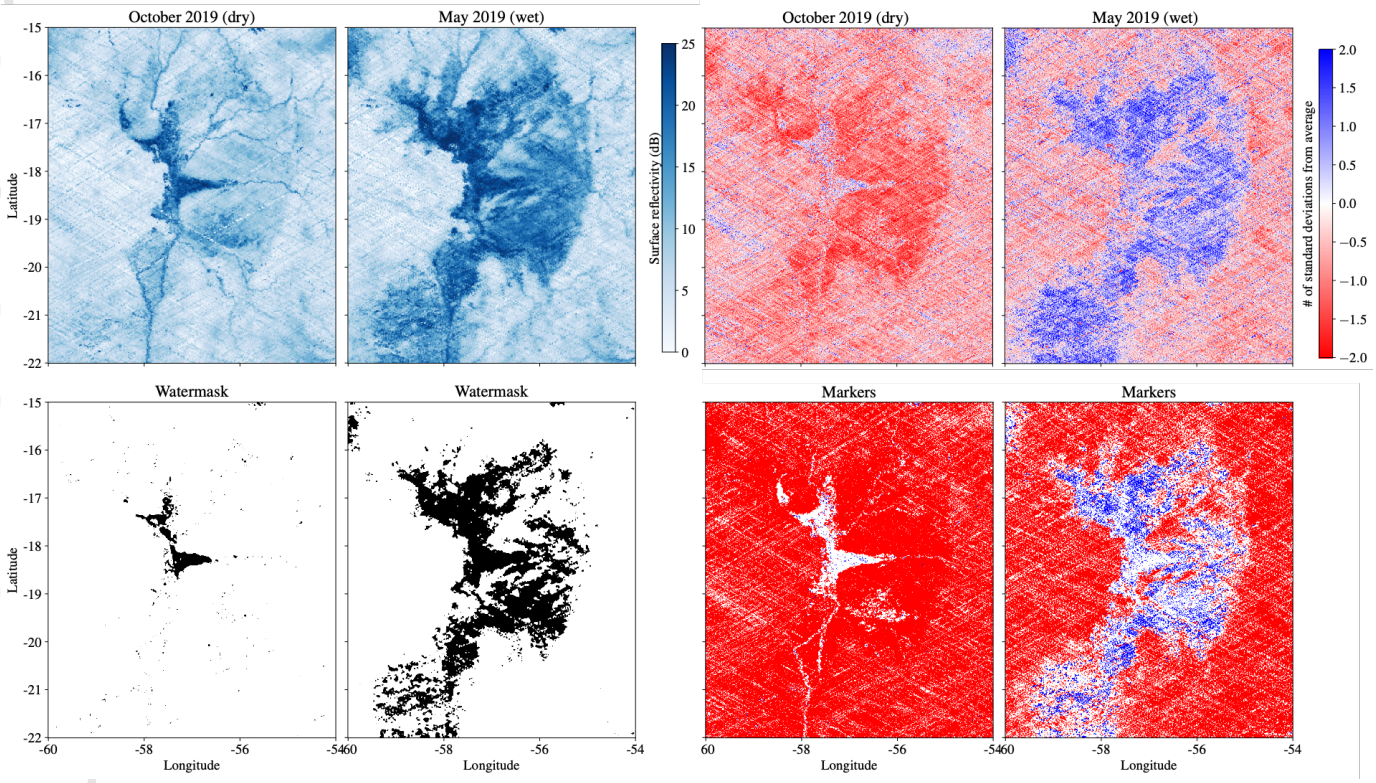

Figure 1: *Algorithm steps applied to two different months of data over the Pantanal: October 2019 (dry season), and May 2019 (wet season). Top left: surface reflectivity from CYGNSS, bottom left: final watermask obtained. Top right: map of the number of standard deviations above or below the 2.5 year average for each individual pixel. Bottom right: markers for the random walker algorithm: red are dry, blue are wet, and white are unassigned pixels.*

2.1.2 Algorithm steps

We start by gridding all the data from years 2017, 2018, and 2019 into a $0.01° \times 0.01°$ grid. Each grid cell contains the whole distribution of CYGNSS overpasses that fell into that gridcell, producing a data cube, where the third dimension contains all the SR data accumulated at each gridcell over two and half year. Because of the CYGNSS' orbit, the sampling density is highest at the edges of CYGNSS' latitudinal band (around 38°N and 38°S) and lowest at the Equator [Bussy-Virat et al., 2019]. The average number of samples in a single grid-cell is 11, ranging from 0 to 40, but with only 0.03% of pixels being actually empty.

We then grid monthly CYGNSS data into the same $0.01° \times 0.01°$ grid, making monthly SR maps from June 2017 until August 2020 (see Figure 1, top left). If a pixel has more than one sample associated with it, the SR value is set to the average of all samples falling within that pixel. SR values above 40 dB are filtered out as they appear to be mostly linked to specific tracks with variations in GPS satellite transmitted power, an issue that is expected to disappear with the upcoming v3 of the CYGNSS data. Using a nearest neighbor interpolation (SciPy, https://scipy.org/), we fill in any pixel without data. We then compare the value of each individual pixel for that month to the average and the standard deviation (STD) of the values for that pixel to produce maps of the number of STDs from the average (Figure 1, top right). In the final step, we use the random walker segmentation from the *scikit-image* library (https://scikit-image.org/) for Python [van der Walt et al., 2014]. This computer vision technique is particularly recommended to segment noisy images [Grady, 2006] and has previously been successfully applied to CYGNSS data [Gerlein-Safdi & Ruf, 2019]. Here, *water* markers are set as pixels that are both one STD above the average for that pixel (over the 2.5 years of data) and that have a SR of at least 18 dB. *Dry* pixels are defined as pixels that are below the average for that pixel and that have a SR below 15 dB (Figure 1, bottom left).

The diffusion parameter of the *scikit-image* function is set to 0.5 and the *wet* and *dry* markers are then allowed to diffuse in random directions, diffusing further in directions with small variations in STD, and stopping when they encounter a sharp gradient. The remaining unassigned pixels are attributed to the *wet* and *dry* categories depending on what labeled marker has the highest probability to reach it first. Figure 1 shows the different steps of the algorithm over the Pantanal during a dry and a wet month and Figure 2 shows two examples of SR maps and final watermasks over the Sudd wetlands.

Looking at the coherence of the signal, it has been established that coherent reflections from water bodies can have a range of SR values, depending on the topography, vegetation cover, and water surface roughness due to wind [Loria et al., 2020]. For this reason, it is key that our technique is actually based on STD maps for a given month, and not on the actual SR data. This allows the random walker algorithm to link together water pixels clearly identified as such, based on both their position within the distribution and their SR values, with unassigned pixels that might have low SR values but can be identified as *wet* from their high values in STD space.

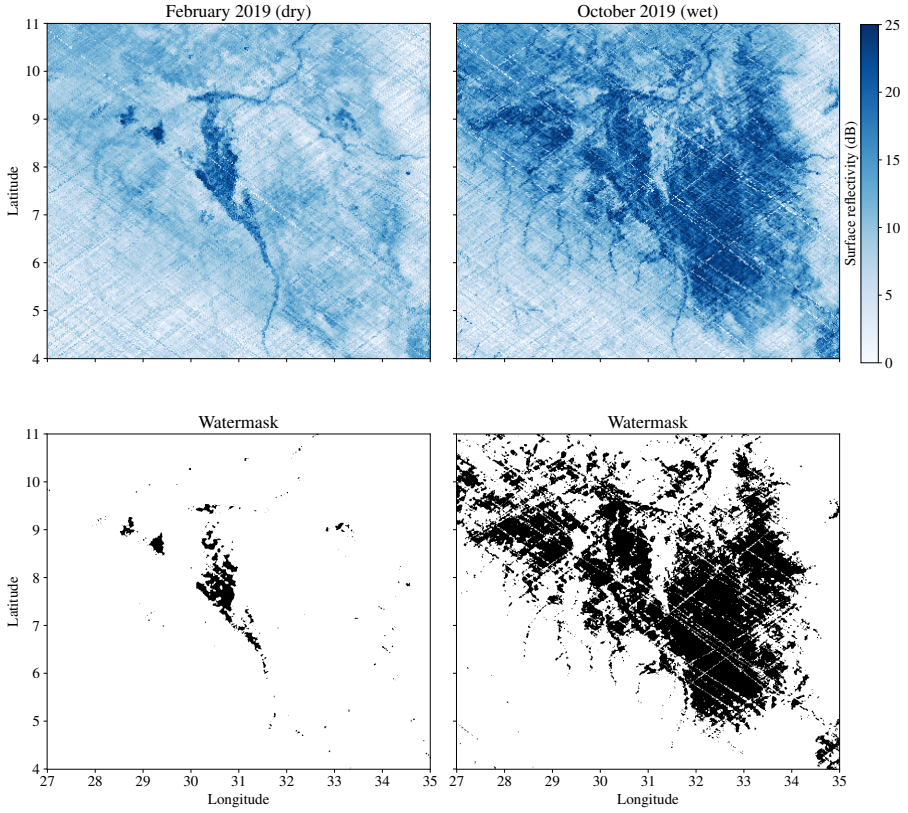

Figure 2: *Inundation maps over the South Sudanese Sudd wetland for two different months of data ; left: February 2019 (dry season), and right: October 2019 (wet season). Top: surface reflectivity from CYGNSS. Bottom: final watermask obtained.*

2.2 WetCHARTs model

2.2.1 Model description

The WetCHARTs model was developed in 2017 [Bloom et al., 2017] to model methane emissions from wetlands globally that are then incorporated into atmospheric chemical transport models. The original model includes three temperature dependence parameterizations of CH_4 respiration fraction and nine heterotrophic respiration simulations (eight carbon cycle models derived from the Multi-scale Synthesis and Terrestrial Model Intercomparison Project and one

data-constrained terrestrial carbon cycle analysis based on the global CARbon DAta MOdel fraMework (CARDAMOM)) for a total of 18 different models for the extended ensemble. The model outputs monthly methane emission estimates at a $0.5^\circ \times 0.5^\circ$ resolution. The standard version of WetCHARTs uses static wetland extent maps based on the Globcover wetland and freshwater land cover types [Bontemps et al., 2011] combined with the the Global Lakes and Wetlands Database (GLWD) [Lehner & Döll, 2004]. Seasonal variations are introduced using either ECMWF Re-Analysis (ERA) rainfall data so that the monthly wetland extent is estimated as:

$$\text{Monthly extent } [\text{m}^2] = \text{static wetland extent } [\text{m}^2] \times \text{precipitation anomaly [unitless]},$$

where the precipitation anomaly is the ratio of the monthly precipitation to mean or max precipitation, depending on whether the static wetland map provides a maximum or mean wetland extent estimate.

Here, we use WetCHARTs version 1.3.1 and we introduce the CYGNSS-based inundation maps as a direct source of information for monthly inundation extent. For this purpose, the CYGNSS maps are downscaled to match WetCHARTs coarser resolution: the maps generated give a fractional water percentage that corresponds to the percentage of the $0.01^\circ \times 0.01^\circ$ pixels within a $0.5^\circ \times 0.5^\circ$ that are marked as *flooded* in the CYGNSS watermasks [Gerlein-Safdi & Ruf, 2021]. These inundation maps are available for download on Zenodo (https://doi.org/10.5281/zenodo.5621107). The full extended ensemble of 18 models is run for the June 2017 to December 2019 period using 1) ERA5 (see Section 2.2.2) rainfall data combined with the static wetland maps from Globcover and GLWD, 2) the dynamic CYGNSS-based inundation maps, and 3) the SWAMPS v3 wetland maps (see Section 2.2.3) that have so far been the standard dynamic inundation maps used to drive WetCHARTs [Zhang et al., 2017a, Pandey et al., 2020, Saunois et al., 2020].

2.2.2 ERA5 rainfall

The ERA5 rainfall dataset is used both in direct comparison with the inundation maps produced by CYGNSS and as a parameter for the WetCHARTs methane emissions. ERA5 combines historical observations into global estimates using advanced modeling and data assimilation systems. In particular, we use monthly rainfall estimates from June 2017 to April 2020 at a 30km grid resolution. The data is regridded to $0.5^\circ \times 0.5^\circ$ resolution when used as an input for WetCHARTs. All ERA5 data is free and available for download on the European Centre for Medium-Range Weather Forecasts website (https://www.ecmwf.int/).

2.2.3 SWAMPS

The SWAMPS wetland maps product was first released in 2015 [Schroeder et al., 2015] and provides maps of fractional surface water globally at 25 km resolution. The product combines active microwave scatterometer data from ERS, QuikSCAT, and ASCAT (each covering a different time period) with radiometer data from SSM/I and SSMI/S (again covering different time periods), environmental variables such as wind speed and precipitation from MERRA-2, and MODIS land cover types maps. Version 3 of the SWAMPS product was released in 2019 [Jensen & Mcdonald, 2019]. The update extends the dataset until 2019, includes more dynamic land cover types, and improves the masking of surfaces types that might raise false positives (such as flat deserts or snow). The data is available freely for download on the website of the Alaska Satellite Facility (https://asf.alaska.edu). Because of the high frequency of the scatterometers used to detect waterbodies, the product is not recommended for use over canopy-obscured wetlands [Schroeder et al., 2015]. Despite this, the SWAMPS maps have been used extensively in WetCHARTs as a driver of wetland extent dynamics [Zhang et al., 2017a, Pandey et al., 2020, Saunois et al., 2020], using the maps to inform relative change compared to the baseline provided by GLWD and GLlobcover. Here, we use SWAMPS v3.2 [Jensen & Mcdonald, 2019] to understand the added value contained in CYGNSS-based inundation maps.

3 Results

3.1 CYGNSS–based monthly watermasks

3.1.1 Spatial patterns

Monthly watermasks are produced for the Pantanal (Figure 1 and S1) and the Sudd (Figure 2 and S2) wetlands at $0.01^\circ \times 0.01^\circ$ resolution. The inundation maps show strong seasonal dynamics, with a significant increase in the extent of the inundated area during the wet season over both the Pantanal and the Sudd. Over the Pantanal during the dry season, the

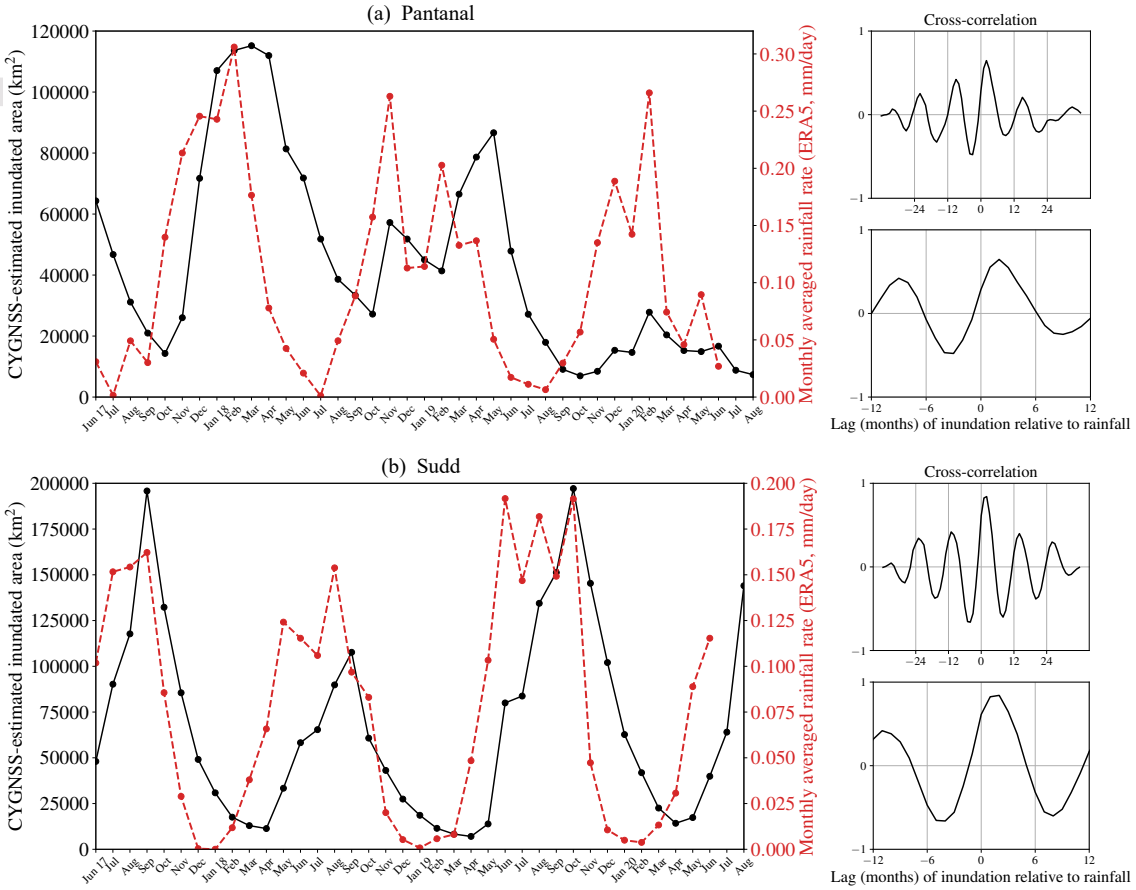

Figure 3: *Monthly inundation extent (black solid lines) based on CYGNSS watermasks and monthly average rainfall rate from ERA-5 data (red dashed line) over (a) the Pantanal and (b) the Sudd. The figures on the right show the cross-correlations between rainfall and inundation extent, highlighting the one to two month lag between the two timeseries.*

maps show an inundation extent similar to that captured by the Global Surface Water Landsat-based product ([Pekel et al., 2016], Figure S3). However, during the wet season, during which the land surface is often invisible to Landsat because of cloud cover, the CYGNSS-based maps show a much larger inundated area. Over the Sudd, the CYGNSS-based data indicate a much larger inundated area than the Global Surface Water product during both the dry and the wet seasons. Note that the white streaks in the final watermasks are associated with large variations in GPS antenna gain that lead to occasional overpasses with very high SNR. This issue has been fixed in the version 3.0 of the CYGNSS data, released at the end of 2020.

3.1.2 Seasonal dynamics

The expected correlation between rainfall amount and inundation extent is apparent when comparing rainfall data to the CYGNSS inundation maps. The direct link between inter-seasonal variations in rainfall amount and the resulting extent of the wetlands is particularly striking when looking at the timeseries of inundation extent (Figure 3) averaged over the entire areas shown in Figures 1 and 2. A cross-correlation analysis shows that the seasonality of rainfall and inundation extent are highly correlated, with a maximum correlation coefficient of 0.84 in the Sudd and 0.65 over the Pantanal. At both locations, this maximum is obtained for a two month lag in inundation compared to rainfall (Figure 3).

In addition, we find that inundation extent demonstrates more inter-seasonal variability than the rainfall rate: both locations

exhibit similar seasonal minimum and maximum rainfall rates, but the effect of small inter-seasonal variations in rainfall appear to have an amplified impact on inundation extent. For example in the Sudd, the 2018 wet season saw a close to 15% decrease in peak rainfall compared to 2017, but peak inundation was only half the acreage of the 2017 peak area (Figure 3). In the Pantanal, the maximum inundation extent during the 2019/2020 wet season only reached about 20% of the 2017/2018 levels.

3.2 Methane emissions from tropical wetlands

The WetCHARTs extended ensemble is run using ERA5 rainfall data, the SWAMPS fractional water maps, and the CYGNSS-based inundation maps from June 2017 to December 2019.

3.2.1 Comparison to rainfall-based emissions

A first order comparison shows that the CYGNSS-based and rainfall-based modeled emissions at both locations display similarly marked seasonality (Figure 4). However, at both locations we find that inundation-driven emissions are systematically higher than rainfall-driven emissions. In particular, rainfall-driven emissions fall to 0 for several months during the dry season, whereas inundation-based emissions are still positive during the dry season and as high as 20 mg CH_4/m^2/day over the Pantanal in 2018.

In addition, we find that the use of CYGNSS-based watermasks shifts both the timing and the magnitude of the methane emissions when compared to the rainfall-driven emissions (Figure 4): similarly to inundation and rainfall, inundation-driven emissions exhibit more inter-seasonal variability than rainfall-driven emissions. A cross-correlation analysis shows that the seasonality of inundation-driven methane emissions is delayed by two month compared to rainfall-driven emissions (Figure 5, peak correlation coefficient in the Sudd: 0.74, in the Pantanal: 0.85), matching the delayed observed between CYGNSS-based inundation timeseries and ERA5 rainfall data (Figure 3).

Maps of the emissions (Figure S5) show that over the Pantanal, the main area driving the difference between rainfall- and inundation-based emissions during the wet season is the south-eastern part of the wetland. Over the Sudd (Figure S6), inundation-based emissions during the wet season are consistently larger than rainfall-driven ones over the eastern side of the wetland.

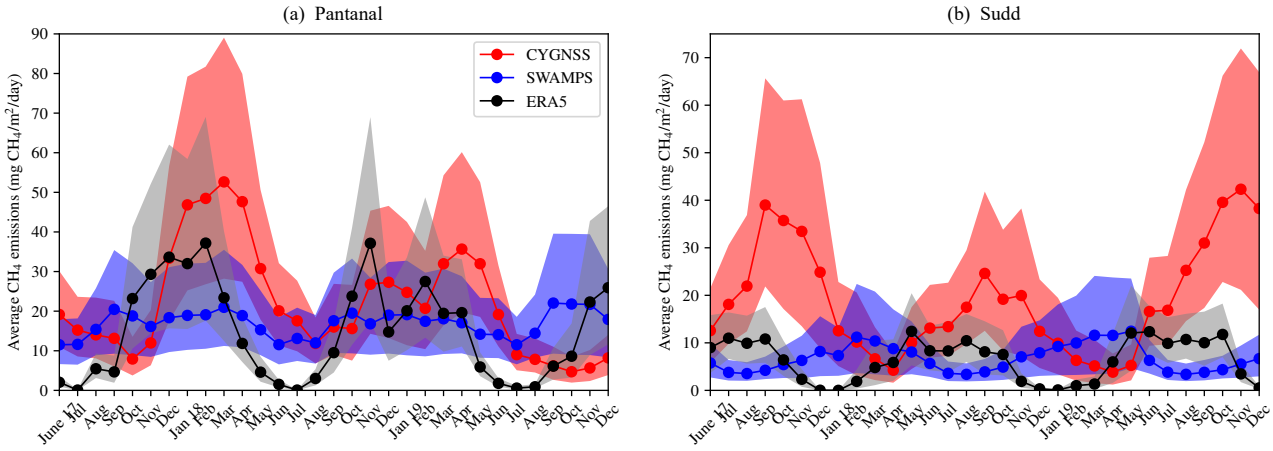

Figure 4: *Average monthly emissions over the whole area for (a) the Pantanal and (b) the Sudd wetlands based on CYGNSS watermasks (red), SWAMPS wetland maps (blue), and ERA5 rainfall (black). Dotted lines are the average of all 18 models and the shaded areas shows the spread between the 5th and the 95th percentiles.*

3.2.2 Comparison to SWAMPS-based emissions

We find that the range of seasonal variation in the SWAMPS maps is much smaller than the CYGNSS maps, which is reflected in the smaller range of variation in the modeled emissions at both locations (Figure 4). In particular, we find that the maximum SWAMPS-based emissions are close to CYGNSS-based lowest emissions. The seasonality of SWAMPS-based emissions matches closely the rainfall-based ones in the Pantanal, but are three to four months early in the Sudd (Figure 4). Emissions maps (Figure S6) indicate that SWAMPS-based emissions are concentrated over the White Nile, at the center of the domain, whereas CYGNSS and rainfall-based emissions are contributed mostly from the western side of the wetland.

4 Discussion

4.1 Hydrological response of wetlands

The CYGNSS satellite constellation provides a new, unique view of two tropical wetlands and their seasonal changes over the last three years. We find that both the Pantanal and the Sudd wetlands exhibit a clear response to the rainfall amount of their wet seasons (Figure 3). While the inundated area peaks about two months after peak rainfall, there are clear spatial patterns in the timing of the flooding that are apparent from Figures S1 and S2. Over the Pantanal, flooding starts early in the rain season along the three main rivers draining into the wetlands: the Cuiabá River to the North, the Taquari River in the Center, and the Rio Negro to the South. In situ measurements along these main rivers also show that the timing of inundation is synchronous to rainfall [da Silva et al., 2020]. The rest of the wetlands fills in, ending with the area along the Paraguay River in the South. In the Sudd, inundation appears to be more homogeneous throughout the valley, although the contribution from the many small tributaries in the western plateau becomes increasingly apparent as the rain season evolves. The time lag found also matches with [Prigent et al., 2020] results over tropical wetlands.

Another interesting feature of the inundation timeseries (Figure 3) is that inundation extent is not only affected by wet season rain, but also dry season rain: this is especially evident during the last rainy season (winter 2019/2020) over the Pantanal during which the wetland stayed mostly dry despite a robust rainy season. This might be tied to the extremely dry season in summer 2019, with nearly no rain from June to September of that year, and that lead to unprecedented wild fires in September through November 2019 [Ionova, 2020]. In-situ data from river gauges indicate that rivers across the wetland were significantly lower than average during the wet season 2019/2020, as well as during the subsequent dry season of 2020 [Marengo et al., 2021]. The drought and post-fire hydrophobicity might have lead to increased surface runoff [Larsen et al., 2009] at the onset of the rainy season and decreased refilling of the wetland as a result, although the very flat topography of wetlands is also expected to limit runoff. Increased infiltration due to drier soils is also possible, but no data was available to confirm either hypotheses.

One limitation of the CYGNSS-based maps is that it is unclear whether the method is capable of differentiating between saturated soils and actual standing water above the soil surface. This is in large part due to the lack of other datasets (in-situ or remotely sensed) that would allow us to validate the maps. However, while this remains an important question to use this data in other contexts, the inundation proxy generated from CYGNSS still provides an informative tool for wetland methane emissions. Indeed, since the L-band probes c. 5-10 cm depth in the soil, signals that are interpreted as inundated may represent total saturation at this depth instead of standing water. This is the depth at which biogeochemical processes are understood to drive methane production [Angle et al., 2017, Zhao et al., 2020] and evidence shows that the effect of water level on wetland methane emissions is non-linear [Shao et al., 2017, de Vicente, 2021], with only negligible differences in emissions between fully saturated and inundated soils.

Finally, because the algorithm looks for times when a pixel has a higher SR value than average, the algorithm is especially suited to capture seasonal wetlands. Permanent wetlands for which pixels are always flooded and the SR always high will tend to be missed by the algorithm, as can be seen in Figure 1: the Paraguay River that flows directly south of the Pantanal is clearly seen in the SR map (Figure 1, top left) but does not get flagged as *wet* because the pixels over the river always have high SR. As a result, the river gets mostly missed in the final watermask (Figure 1, bottom left). However, many high resolution maps exist for permanent water bodies since their position is stable and therefore better known than that of seasonal wetlands. Datasets such as the ones proposed in [Pekel et al., 2016], [Yamazaki et al., 2019], or [Lin et al., 2021] are all potential candidates that we are planning to leverage to complement the current algorithm as we expend it to the entire CYGNSS latitudinal range (c. 40°N to 40°S).

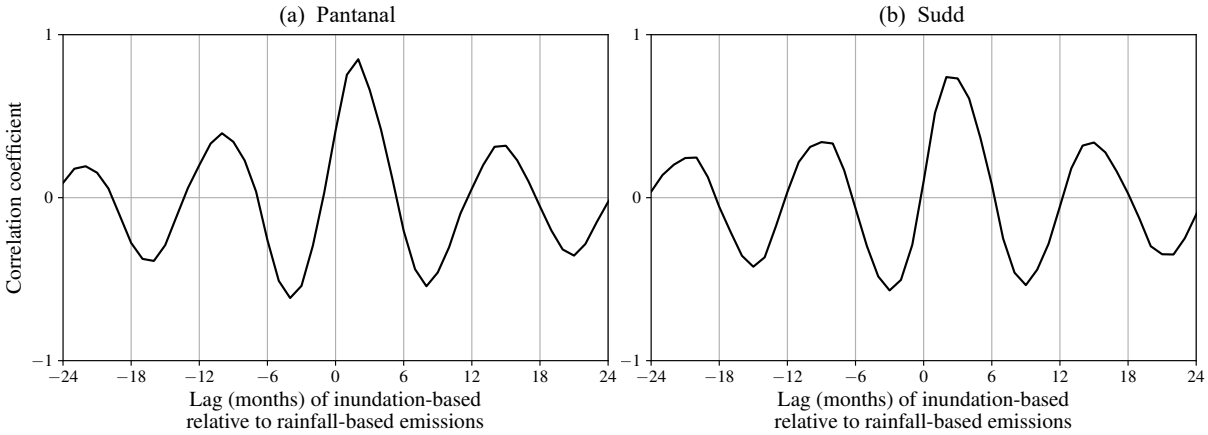

Figure 5: *Cross-correlations between rainfall-based and inundation-based WetCHARTs CH_4 emissions, highlighting the two months lag between the two timeseries over (a) the Pantanal and (b) the Sudd wetlands.*

4.2 Impact of CYGNSS-based watermasks on modeled methane emissions

The WetCHARTs model is a unique tool to understand what drives wetland methane emissions and how wetlands contribute to the global methane cycle.

4.2.1 Improvements of CYGNSS maps over existing products

The observed discrepancy in seasonality in SWAMPS-based emissions over the Sudd matches the results from [Pandey et al., 2020], which found that SWAMPS maps over the Sudd wetlands are more than three months ahead of the seasonality in rainfall and TROPOMI total column methane observations. They found that the SWAMPS seasonality was instead closely aligned with river height of the White Nile. This matches our results that showed that SWAMPS-based emissions where predominantly coming from the White Nile (Figure S6). [Pandey et al., 2020]. [Pandey et al., 2020] attributes the discrepancy to SWAMPS' incapacity to map wetlands under vegetation [Schroeder et al., 2015]. This result along with the smaller wetland area estimates, that lead to significantly lower modeled methane emissions, confirm that high frequency microwave data, such as the one used for SWAMPS are not appropriate to map tropical wetlands accurately due to the presence of vegetation, but that CYGNSS data can help fill in this data gap.

4.2.2 Assessing CYGNSS-based modeled emissions

While the Pantanal and the Sudd are located in remote areas where in-situ data is sparse, we do have a few pieces of evidence indicating that inundation-based modeled emissions are in better agreement with measured fluxes.

First, one of the striking characteristics of the rainfall-driven model is the absence of methane emissions during the dry season at both the Pantanal and the Sudd. In contrast, inundation-driven maps show a reduced but still significant flux during the dry season, corresponding to 0.1 to 0.3 Tg CH_4/month in the Pantanal and 0.05 to 0.1 Tg CH_4/month in the Sudd (Figure S4). Flux tower measurements made in the Pantanal between 2014 and 2017 [Dalmagro et al., 2019] confirm that the wetland effluxes CH_4 even during the dry season. Here, we find that the residual fluxes are mainly coming from the western part of the wetlands (Figure S5) that is considered to be inundated year-round.

Secondly, using the Japanese Greenhouse gases Observing Satellite (GOSAT) over the Sudd wetlands, [Lunt et al., 2019] found yearly emissions ranging from about 2.5 to 7 Tg/year between 2010 and 2016. We find that in 2018, the average yearly emissions for the rainfall-based WetCHARTs models was 1.09 ± 0.50 Tg (average across all 18 models ± standard deviation) and 1.23 ± 0.48 Tg in 2019 (Figure S4). For the inundation-based models, the average was 2.10 ± 0.94 Tg in 2018 and 3.58 ± 1.43 Tg in 2019. While we only have a short timeseries, both the higher average and the larger range of year-to-year variation of the inundation-based emissions are in better agreement with the GOSAT analysis than are the rainfall-based emissions.

Third, [Parker et al., 2018] found that the GOSAT total column methane over the Pantanal peaks about one month later than the rainfall-based WetCHARTs model. This delay is even clearer over the Paraná river in Argentina and this result is consistent with the delay we observed between rainfall-driven and inundation-driven emissions (Figure 5).

Lastly, [Pandey et al., 2020] showed that over the Sudd wetlands, methane emissions models and methane concentrations measured from the TROPOspheric Monitoring Instrument (TROPOMI, [Hu et al., 2018]) are out-of-sync. The authors came to the conclusion that the mismatch was due to a an issue with wetland extent maps and the discrepancy between rainfall and surface inundation, a result that is indeed confirmed by our study.

4.3 Consequence for global methane emissions

Wetlands are the largest natural emitters of methane and these emissions will likely increase with increasing temperatures due to climate change [Zhang et al., 2017b]. Understanding how methane will influence climate change and producing more accurate climate models is therefore dependent on improving our methane emissions models. Wetland extent has been identified time and time again as the largest source of uncertainty [Zhang et al., 2017a, Turner et al., 2019, Parker et al., 2020] and our work introduces a new, robust method for mapping wetlands based on CYGNSS data. The range of evidence coming from both the Sudd and the Pantanal indicates that these new inundation maps produce emissions that better capture the average and the temporal dynamics of both in-situ and remotely-sensed methane fluxes. This is crucial since many recent studies are finding that models are performing poorly at capturing the timing and the seasonal range of variations in wetland emissions when compared to new satellite methane data that has been becoming available [Parker et al., 2018, Lunt et al., 2019, Pandey et al., 2020]. Here, we demonstrated that what the community needs to significantly improve emissions models is more accurate wetland maps that are able to accurately capture the full range of variation in wetland extent.

The CYGNSS-based wetland mapping technique presented here is currently being extended to the full CYGNSS coverage, about 40°N and 40°S, and could help improve wetland emissions models in this latitudinal range. However, how this new information will influence global emissions is not clear.On the one hand, our results indicate that improved inundation maps would lead to an overall increase in predicted wetland emissions during both the dry and wet seasons. On the other hand, evidence from the Pantanal shows that in some wetlands, there is more inter-seasonal variation in inundation than there is in rainfall, sometimes leading to a smaller-than-average wetland area even when rainfall amount is normal [Sandi et al., 2020]. This is due to the wetlands' response to both wet and dry season rainfall, as well as upstream precipitation [Fossey et al., 2016, Karim et al., 2016]. Because existing wetland maps have been failing at capturing intra-seasonal dynamics, very little is know about the seasonal cycle of individual wetlands and their response to year-to-year variations in rainfall and evaporative conditions. However, accurately representing the wetland response to interannual variations in precipitation and temperature is the first step to properly characterize the effects that climate change will have on these ecosystems. In addition, the increasing pressure that many tropical ecosystems are facing from both land use change and climate change-induced increases in rainfall variability is likely to lead to a global reduction in wetland extent in the long run [Junk, 2002, Dixon et al., 2016, Inogwabini, 2020]. This would in turn drive a decrease in methane emissions. For this reason,the high quality maps of wetlands at high temporal and spatial resolution and unaffected by clouds or vegetation that we developed here based on CYGNSS data will be crucial to resolve seasonal dynamics [Rajib et al., 2020] and understand the resulting methane emissions and their sensitivity to variations in temperature and precipitation.

5 Conclusion

Wetlands are the largest natural source of methane on the planet. Uncertainty associated with wetland extent and tropical wetlands in particular is a leading source of inconsistency between models and existing data, an issue that the CYGNSS satellite data can help improve on. By providing monthly maps of inundated land at $0.01° \times 0.01°$, we were able to capture wetlands seasonal dynamics and their response to wet and dry season rainfall input. We focused on two of the largest tropical wetlands: the Pantanal in Brazil and the Sudd in South Sudan. The new CYGNSS-based maps were incorporated into the WetCHARTs wetland methane emissions model and the results compared to WetCHARTs standard input that uses ERA5 rainfall data. We found that the inundation-based emissions have a seasonality shifted by about two months compared to the rainfall-driven emissions. In addition, dry season inundation-driven emissions were consistently

higher in both locations. Finally, we found that inundation experiences more inter-seasonal variability than rainfall does, resulting in more variable emissions for the inundation-driven models than for the rainfall-driven version. These results highlight the need to generate and include better wetland maps into emissions models in order to get an accurate picture of the effects of methane on climate change.

Acknowledgment

This work was supported in part by a fellowship from the Michigan Society of Fellows and by a NASA Science Mission Directorate contract NNL13AQ00C with the University of Michigan. Part of this research was carried out at the Jet Propulsion Laboratory, California Institute of Technology under a contract with the National Aeronautics and Space Administration. Funding for the WetCHARTs emissions was provided through a NASA Carbon Monitoring System Grant NNH14ZDA001N-CMS.

Data availability

- The CYGNSS data used in this article (doi: 10.5067/CYGNS-L1X21) are publicly available from the NASA Physical Oceanography Distributed Active Archive Center at the following link: `https://podaac.jpl.nasa.gov/dataset/CYGNSS_L1_V2.1`.
- The CYGNSS-based inundation maps of the Sudd and the Pantanal produced for this project (doi: 10.5281/zenodo.5621107) and used in WetCHARTs are available on Zenodo at the following link: `https://doi.org/10.5281/zenodo.5621107`.
- The WetCHARTs model results (doi: 10.3334/ORNLDAAC/1502) are accessible through the Oak Ridge National Laboratory Distributed Active Archive Center at the following link: `https://daac.ornl.gov/cgi-bin/dsviewer.pl?ds_id=1502`.
- The ERA5 monthly averaged rainfall data (doi: 10.24381/cds.68d2bb30) is available from the Copernicus website as part of the ERA5-Land data at the following link: `https://doi.org/10.24381/cds.68d2bb30`.
- The Global Surface Water product (source: EC JRC/Google) used to generate Figure S3 is publicly available from the Global Water Surface Explorer website at the following link: `https://global-surface-water.appspot.com/`
- The SWAMPS data is available freely for download on the website of the Alaska Satellite Facility at the following link: `https://asf.alaska.edu/data-sets/derived-data-sets/wetlands-measures/`.

References

[Al-Khaldi et al., 2020] Al-Khaldi, M. M., Johnson, J. T., Gleason, S., Loria, E., O'Brien, A. J., & Yi, Y. (2020). An Algorithm for Detecting Coherence in Cyclone Global Navigation Satellite System Mission Level-1 Delay-Doppler Maps. *IEEE Transactions on Geoscience and Remote Sensing*, doi:10.1109/TGRS.2020.3009784.

[Angle et al., 2017] Angle, J. C., et al. (2017). Methanogenesis in oxygenated soils is a substantial fraction of wetland methane emissions. *Nature Communications*, *8*(1), 1567, doi:10.1038/s41467-017-01753-4.

[Bloom et al., 2017] Bloom, A., et al. (2017). A global wetland methane emissions and uncertainty dataset for atmospheric chemical transport models (WetCHARTs version 1.0). *Geoscientific Model Development*, *10*(6), 2141–2156, doi:10.5194/gmd-10-2141-2017.

[Bontemps et al., 2011] Bontemps, S., Defourny, P., Bogaert, E. V., Arino, O., Kalogirou, V., & Perez, J. R. (2011). *Globcover products description and validation report*. Technical report, European Space Agency.

[Bussy-Virat et al., 2019] Bussy-Virat, C. D., Ruf, C. S., & Ridley, A. J. (2019). Relationship between Temporal and Spatial Resolution for a Constellation of GNSS-R Satellites. *IEEE Journal of Selected Topics in Applied Earth Observations and Remote Sensing*, *12*(1), 16–25, doi:10.1109/JSTARS.2018.2833426.

[Camps, 2020] Camps, A. (2020). Spatial Resolution in GNSS-R Under Coherent Scattering. *IEEE Geoscience and Remote Sensing Letters*, *17*(1), 32–36, doi:10.1109/LGRS.2019.2916164.

[Carreno-Luengo et al., 2020] Carreno-Luengo, H., Luzi, G., & Crosetto, M. (2020). Above-Ground Biomass Retrieval over Tropical Forests: A Novel GNSS-R Approach with CyGNSS. *Remote Sensing*, *12*(9), 1368, doi:10.3390/rs12091368.

[Chew et al., 2018] Chew, C., Reager, J. T., & Small, E. (2018). CYGNSS data map flood inundation during the 2017 Atlantic hurricane season. *Scientific Reports*, *8*(1), 9336, doi:10.1038/s41598-018-27673-x.

[Chew & Small, 2020] Chew, C. & Small, E. (2020). Estimating inundation extent using CYGNSS data: A conceptual modeling study. *Remote Sensing of Environment*, *246*(January), 111869, doi:10.1016/j.rse.2020.111869.

[Chew & Small, 2018] Chew, C. C. & Small, E. E. (2018). Soil Moisture Sensing Using Spaceborne GNSS Reflections: Comparison of CYGNSS Reflectivity to SMAP Soil Moisture. *Geophysical Research Letters*, *45*(9), 4049–4057, doi:10.1029/2018GL077905.

[Ciais et al., 2013] Ciais, P., et al. (2013). *Climate Change 2013: the physical science basis. Contribution of working group I to the fifth assessment report of the Intergovernmental Panel on Climate Change*, chapter Carbon and Other Biogeochemical Cycles, (pp. 465–570). Cambridge University Press, Cambridge, United Kingdom and New York, NY, USA.

[da Silva et al., 2020] da Silva, B., Henrique, F., da Cunha, C. N., & Overbeck, G. E. (2020). Seasonal Dynamics of Flooded Tropical Grassland Communities in the Pantanal Wetland. *Wetlands*, doi:10.1007/s13157-020-01281-w.

[Dalmagro et al., 2019] Dalmagro, H. J., Zanella de Arruda, P. H., Vourlitis, G. L., Lathuillière, M. J., de S. Nogueira, J., Couto, E. G., & Johnson, M. S. (2019). Radiative forcing of methane fluxes offsets net carbon dioxide uptake for a tropical flooded forest. *Global Change Biology*, *25*(6), 1967–1981, doi:10.1111/gcb.14615.

[de Vicente, 2021] de Vicente, I. (2021). Biogeochemistry of Mediterranean Wetlands: A Review about the Effects of Water-Level Fluctuations on Phosphorus Cycling and Greenhouse Gas Emissions. *Water*, *13*(11), 1510, doi:10.3390/w13111510.

[Dixon et al., 2016] Dixon, M., Loh, J., Davidson, N., Beltrame, C., Freeman, R., & Walpole, M. (2016). Tracking global change in ecosystem area: The Wetland Extent Trends index. *Biological Conservation*, *193*, 27–35, doi:10.1016/j.biocon.2015.10.023.

[Fletcher & Schaefer, 2019] Fletcher, S. E. M. & Schaefer, H. (2019). Rising methane: A new climate challenge. *Science*, *364*(6444), 932–933, doi:10.1126/science.aax1828.

[Fossey et al., 2016] Fossey, M., Rousseau, A., & Savary, S. (2016). Assessment of the impact of spatio-temporal attributes of wetlands on stream flows using a hydrological modelling framework: a theoretical case study of a watershed under temperate climatic conditions. *Hydrological Processes*, *30*(11), 1768–1781, doi:10.1002/hyp.10750.

[Ganesan et al., 2019] Ganesan, A. L., et al. (2019). Advancing Scientific Understanding of the Global Methane Budget in Support of the Paris Agreement. *Global Biogeochemical Cycles*, *33*(12), 1475–1512, doi:10.1029/2018GB006065.

[Gerlein-Safdi & Ruf, 2021] Gerlein-Safdi, C. & Ruf, C. (2021). CYGNSS-based inundation maps of the Pantanal and the Sudd wetlands from June 2017 to December 2019.

[Gerlein-Safdi & Ruf, 2019] Gerlein-Safdi, C. & Ruf, C. S. (2019). A CYGNSS-Based Algorithm for the Detection of Inland Waterbodies. *Geophysical Research Letters*, *46*(21), 12065–12072, doi:10.1029/2019GL085134.

[Grady, 2006] Grady, L. (2006). Random Walks for Image Segmentation. *IEEE Transactions on Pattern Analysis and Machine Intelligence*, *28*(11), 1768–1783, doi:10.1109/TPAMI.2006.233.

[Hess et al., 2015] Hess, L. L., Melack, J. M., Affonso, A. G., Barbosa, C., Gastil-Buhl, M., & Novo, E. M. (2015). Wetlands of the Lowland Amazon Basin: Extent, Vegetative Cover, and Dual-season Inundated Area as Mapped with JERS-1 Synthetic Aperture Radar. *Wetlands*, *35*(4), 745–756, doi:10.1007/s13157-015-0666-y.

[Hu et al., 2018] Hu, H., et al. (2018). Toward Global Mapping of Methane With TROPOMI: First Results and Intersatellite Comparison to GOSAT. *Geophysical Research Letters*, *45*(8), 3682–3689, doi:10.1002/2018GL077259.

[Inogwabini, 2020] Inogwabini, B. (2020). The changing water cycle: Freshwater in the Congo. *WIREs Water*, *7*(2), 1–17, doi:10.1002/wat2.1410.

[Ionova, 2020] Ionova, A. (2020). 'Out of control': Unprecedented fires ravage Brazil's Pantanal wetlands. *Mongabay News*.

[Jensen & Mcdonald, 2019] Jensen, K. & Mcdonald, K. (2019). Surface Water Microwave Product Series Version 3: A Near-Real Time and 25-Year Historical Global Inundated Area Fraction Time Series From Active and Passive Microwave Remote Sensing. *IEEE Geoscience and Remote Sensing Letters*, *16*(9), 1402–1406, doi:10.1109/lgrs.2019.2898779.

[Jeziorska, 2019] Jeziorska, J. (2019). UAS for Wetland Mapping and Hydrological Modeling. *Remote Sensing*, *11*(17), 1997, doi:10.3390/rs11171997.

[Junk, 2002] Junk, W. J. (2002). Long-term environmental trends and the future of tropical wetlands. *Environmental Conservation*, *29*(4), 414–435, doi:10.1017/S0376892902000310.

[Karim et al., 2016] Karim, F., Petheram, C., Marvanek, S., Ticehurst, C., Wallace, J., & Hasan, M. (2016). Impact of climate change on floodplain inundation and hydrological connectivity between wetlands and rivers in a tropical river catchment. *Hydrological Processes*, *30*(10), 1574–1593, doi:10.1002/hyp.10714.

[Koffi et al., 2020] Koffi, E. N., Bergamaschi, P., Alkama, R., & Cescatti, A. (2020). An observation-constrained assessment of the climate sensitivity and future trajectories of wetland methane emissions. *Science Advances*, *6*(15), eaay4444, doi:10.1126/sciadv.aay4444.

[Landmann et al., 2010] Landmann, T., Schramm, M., Colditz, R. R., Dietz, A., & Dech, S. (2010). Wide Area Wetland Mapping in Semi-Arid Africa Using 250-Meter MODIS Metrics and Topographic Variables. *Remote Sensing*, *2*(7), 1751–1766, doi:10.3390/rs2071751.

[Larsen et al., 2009] Larsen, I. J., et al. (2009). Causes of Post-Fire Runoff and Erosion: Water Repellency, Cover, or Soil Sealing? *Soil Science Society of America Journal*, *73*(4), 1393–1407, doi:10.2136/sssaj2007.0432.

[Lehner & Döll, 2004] Lehner, B. & Döll, P. (2004). Development and validation of a global database of lakes, reservoirs and wetlands. *Journal of Hydrology*, *296*(1-4), 1–22, doi:10.1016/j.jhydrol.2004.03.028.

[Lin et al., 2021] Lin, P., Pan, M., Wood, E. F., Yamazaki, D., & Allen, G. H. (2021). A new vector-based global river network dataset accounting for variable drainage density. *Scientific Data*, *8*(1), 28, doi:10.1038/s41597-021-00819-9.

[Loria et al., 2020] Loria, E., O'Brien, A., Zavorotny, V., Downs, B., & Zuffada, C. (2020). Analysis of scattering characteristics from inland bodies of water observed by CYGNSS. *Remote Sensing of Environment*, *245*(November 2019), 111825, doi:10.1016/j.rse.2020.111825.

[Lunt et al., 2019] Lunt, M. M., Palmer, P. P., Feng, L., Taylor, C. C., Boesch, H., & Parker, R. R. (2019). An increase in methane emissions from tropical Africa between 2010 and 2016 inferred from satellite data. *Atmospheric Chemistry and Physics*, *19*(23), 14721–14740, doi:10.5194/acp-19-14721-2019.

[Marani & Alvalá, 2007] Marani, L. & Alvalá, P. C. (2007). Methane emissions from lakes and floodplains in Pantanal, Brazil. *Atmospheric Environment*, *41*(8), 1627–1633, doi:10.1016/j.atmosenv.2006.10.046.

[Marengo et al., 2021] Marengo, J. A., et al. (2021). Extreme Drought in the Brazilian Pantanal in 2019–2020: Characterization, Causes, and Impacts. *Frontiers in Water*, *3*(February), doi:10.3389/frwa.2021.639204.

[Martins et al., 2018] Martins, V. S., Novo, E. M., Lyapustin, A., Aragão, L. E., Freitas, S. R., & Barbosa, C. C. (2018). Seasonal and interannual assessment of cloud cover and atmospheric constituents across the Amazon (2000–2015): Insights for remote sensing and climate analysis. *ISPRS Journal of Photogrammetry and Remote Sensing*, *145*(October 2017), 309–327, doi:10.1016/j.isprsjprs.2018.05.013.

[Miller et al., 2013] Miller, S. M., et al. (2013). Anthropogenic emissions of methane in the United States. *Proceedings of the National Academy of Sciences*, *110*(50), 20018–20022, doi:10.1073/pnas.1314392110.

[Mitchard, 2018] Mitchard, E. T. (2018). The tropical forest carbon cycle and climate change. *Nature*, *559*(7715), 527–534, doi:10.1038/s41586-018-0300-2.

[Morris et al., 2019] Morris, M., Chew, C., Reager, J. T., Shah, R., & Zuffada, C. (2019). A novel approach to monitoring wetland dynamics using CYGNSS: Everglades case study. *Remote Sensing of Environment*, *233*(August), 111417, doi:10.1016/j.rse.2019.111417.

[Nghiem et al., 2017] Nghiem, S. V., et al. (2017). Wetland monitoring with global navigation satellite system reflectometry. *Earth and Space Science*, *4*(1), 16–39, doi:10.1002/2016EA000194.

[Nisbet et al., 2019] Nisbet, E. G., et al. (2019). Very Strong Atmospheric Methane Growth in the 4 Years 2014–2017: Implications for the Paris Agreement. *Global Biogeochemical Cycles*, *33*(3), 318–342, doi:10.1029/2018GB006009.

[Pandey et al., 2020] Pandey, S., Houweling, S., Lorente, A., Borsdorff, T., Tsivlidou, M., & Anthony, A. (2020). Using satellite data to identify the methane emission controls of South Sudan's wetlands. *Biogeosciences*, *preprint*, doi:10.5194/bg-2020-251.

[Park et al., 2020] Park, H., Camps, A., Castellvi, J., & Muro, J. (2020). Generic Performance Simulator of Spaceborne GNSS-Reflectometer for Land Applications. *IEEE Journal of Selected Topics in Applied Earth Observations and Remote Sensing*, *13*, 3179–3191, doi:10.1109/JSTARS.2020.3000391.

[Parker et al., 2018] Parker, R. J., et al. (2018). Evaluating year-to-year anomalies in tropical wetland methane emissions using satellite CH_4 observations. *Remote Sensing of Environment*, *211*(April), 261–275, doi:10.1016/j.rse.2018.02.011.

[Parker et al., 2020] Parker, R. J., et al. (2020). Exploring Constraints on a Wetland Methane Emission Ensemble (WetCHARTs) using GOSAT Satellite Observations. *Biogeosciences*, *preprint*, doi:10.5194/bg-2020-284.

[Pekel et al., 2016] Pekel, J. F., Cottam, A., Gorelick, N., & Belward, A. S. (2016). High-resolution mapping of global surface water and its long-term changes. *Nature*, *540*(7633), 418–422, doi:10.1038/nature20584.

[Post et al., 2019] Post, E., et al. (2019). The polar regions in a 2 °C warmer world. *Science Advances*, *5*(12), eaaw9883, doi:10.1126/sciadv.aaw9883.

[Prigent et al., 2020] Prigent, C., Jimenez, C., & Bousquet, P. (2020). Satellite-Derived Global Surface Water Extent and Dynamics Over the Last 25 Years (GIEMS-2). *Journal of Geophysical Research: Atmospheres*, *125*(3), 1–18, doi:10.1029/2019JD030711.

[Prigent et al., 2007] Prigent, C., Papa, F., Aires, F., Rossow, W. B., & Matthews, E. (2007). Global inundation dynamics inferred from multiple satellite observations, 1993–2000. *Journal of Geophysical Research*, *112*(D12), D12107, doi:10.1029/2006JD007847.

[Rajib et al., 2020] Rajib, A., Golden, H. E., Lane, C. R., & Wu, Q. (2020). Surface Depression and Wetland Water Storage Improves Major River Basin Hydrologic Predictions. *Water Resources Research*, *56*(7), 1–19, doi:10.1029/2019WR026561.

[Ruf et al., 2018] Ruf, C. S., Chew, C., Lang, T., Morris, M. G., Nave, K., Ridley, A., & Balasubramaniam, R. (2018). A New Paradigm in Earth Environmental Monitoring with the CYGNSS Small Satellite Constellation. *Scientific Reports*, *8*(1), 8782, doi:10.1038/s41598-018-27127-4.

[Sandi et al., 2020] Sandi, S. G., Rodriguez, J. F., Saintilan, N., Wen, L., Kuczera, G., Riccardi, G., & Saco, P. M. (2020). Resilience to drought of dryland wetlands threatened by climate change. *Scientific Reports*, *10*(1), 13232, doi:10.1038/s41598-020-70087-x.

[Saunois et al., 2016] Saunois, M., et al. (2016). The Global Methane Budget 2000–2012. *Earth System Science Data*, *8*(2), 697–751, doi:10.5194/essd-8-697-2016.

[Saunois et al., 2020] Saunois, M., et al. (2020). The Global Methane Budget 2000–2017. *Earth System Science Data*, *12*(3), 1561–1623, doi:10.5194/essd-12-1561-2020.

[Schroeder et al., 2015] Schroeder, R., et al. (2015). Development and Evaluation of a Multi-Year Fractional Surface Water Data Set Derived from Active/Passive Microwave Remote Sensing Data. *Remote Sensing*, *7*(12), 16688–16732, doi:10.3390/rs71215843.

[Shao et al., 2017] Shao, X., Sheng, X., Wu, M., Wu, H., & Ning, X. (2017). Methane production potential and emission at different water levels in the restored reed wetland of Hangzhou Bay. *PLOS ONE*, *12*(10), e0185709, doi:10.1371/journal.pone.0185709.

[Shen et al., 2019] Shen, X., Anagnostou, E. N., Allen, G. H., Robert Brakenridge, G., & Kettner, A. J. (2019). Near-real-time non-obstructed flood inundation mapping using synthetic aperture radar. *Remote Sensing of Environment*, *221*(November 2018), 302–315, doi:10.1016/j.rse.2018.11.008.

[Treat et al., 2018] Treat, C. C., Bloom, A. A., & Marushchak, M. E. (2018). Nongrowing season methane emissions-a significant component of annual emissions across northern ecosystems. *Global Change Biology*, *24*(8), 3331–3343, doi:10.1111/gcb.14137.

[Turner et al., 2019] Turner, A. J., Frankenberg, C., & Kort, E. A. (2019). Interpreting contemporary trends in atmospheric methane. *Proceedings of the National Academy of Sciences of the United States of America*, *116*(8), 2805–2813, doi:10.1073/pnas.1814297116.

[van der Walt et al., 2014] van der Walt, S., et al. (2014). scikit-image: image processing in Python. *PeerJ*, *2*(1), e453, doi:10.7717/peerj.453.

[Wang & Morton, 2020] Wang, Y. & Morton, Y. J. (2020). Coherent GNSS Reflection Signal Processing for High-Precision and High-Resolution Spaceborne Applications. *IEEE Transactions on Geoscience and Remote Sensing*, (pp. 1–12)., doi:10.1109/TGRS.2020.2993804.

[Yamazaki et al., 2019] Yamazaki, D., Ikeshima, D., Sosa, J., Bates, P. D., Allen, G. H., & Pavelsky, T. M. (2019). MERIT Hydro: A High-Resolution Global Hydrography Map Based on Latest Topography Dataset. *Water Resources Research*, *55*(6), 5053–5073, doi:10.1029/2019WR024873.

[Zhang et al., 2017a] Zhang, B., Tian, H., Lu, C., Chen, G., Pan, S., Anderson, C., & Poulter, B. (2017a). Methane emissions from global wetlands: An assessment of the uncertainty associated with various wetland extent data sets. *Atmospheric Environment*, *165*, 310–321, doi:10.1016/j.atmosenv.2017.07.001.

[Zhang et al., 2017b] Zhang, Z., et al. (2017b). Emerging role of wetland methane emissions in driving 21st century climate change. *Proceedings of the National Academy of Sciences of the United States of America*, *114*(36), 9647–9652, doi:10.1073/pnas.1618765114.

[Zhao et al., 2020] Zhao, M., et al. (2020). Responses of soil CO2 and CH4 emissions to changing water table level in a coastal wetland. *Journal of Cleaner Production*, *269*, 122316, doi:10.1016/j.jclepro.2020.122316.

[Zweig et al., 2015] Zweig, C. L., Burgess, M. A., Percival, H. F., & Kitchens, W. M. (2015). Use of Unmanned Aircraft Systems to Delineate Fine-Scale Wetland Vegetation Communities. *Wetlands*, *35*(2), 303–309, doi:10.1007/s13157-014-0612-4.